Experimental Astronomy manuscript No.
(will be inserted by the editor)

The Large Observatory for X-ray Timing (LOFT)

M. Feroci[⋆,1,73], L. Stella[⋆⋆,2], M. van der Klis[3], T. J.-L. Courvoisier[4], M. Hernanz[5], R. Hudec[6], A. Santangelo[7], D. Walton[8], A. Zdziarski[9], D. Barret[14], T. Belloni[21], J. Braga[26], S. Brandt[27], C. Budtz-Jørgensen[27], S. Campana[21], J.-W. den Herder[38], J. Huovelin[48], G. L. Israel[2], M. Pohl[78], P. Ray[64], A. Vacchi[24], S. Zane[8], A. Argan[74], P. Attinà[15], G. Bertuccio[22], E. Bozzo[4], R. Campana[1,73], D. Chakrabarty[32], E. Costa[1], A. De Rosa[1], E. Del Monte[1,73], S. Di Cosimo[1], I. Donnarumma[1], Y. Evangelista[1], D. Haas[38], P. Jonker[38], S. Korpela[48], C. Labanti[12], P. Malcovati[45], R. Mignani[8,72], F. Muleri[1], M. Rapisarda[75,1,73], A. Rashevsky[24], N. Rea[5], A. Rubini[1,73], C. Tenzer[7], C. Wilson-Hodge[70], B. Winter[8], K. Wood[64], G. Zampa[24], N. Zampa[24], M. A. Abramowicz[10], M.A. Alpar[11], D. Altamirano[3], J. M. Alvarez[5], L. Amati[12], C. Amoros[14], L. A. Antonelli[2], R. Artigue[14], P. Azzarello[4], M. Bachetti[14], G. Baldazzi[16], M. Barbera[17], C. Barbieri[18], S. Basa[19], A. Baykal[20], R. Belmont[14], L. Boirin[23], V. Bonvicini[24], L. Burderi[28], M. Bursa[29], C. Cabanac[14], E. Cackett[30], G. A. Caliandro[5], P. Casella[31], S. Chaty[33], J. Chenevez[27], M. J. Coe[31], A. Collura[17], A. Corongiu[34], S. Covino[21], G. Cusumano[35], F. D'Amico[26], S. Dall'Osso[36], D. De Martino[37], G. De Paris[74], G. Di Persio[1], T. Di Salvo[17], C. Done[39], M. Dovčiak[29], A. Drago[40], U. Ertan[11], S. Fabiani[1], M. Falanga[41], R. Fender[31], P. Ferrando[33], D. Della Monica Ferreira[27], G. Fraser[42], F. Frontera[40], F. Fuschino[12], J. L. Galvez[5], P. Gandhi[43], P. Giommi[44], O. Godet[14], E. Göğüş[11], A. Goldwurm[33], D. Götz[33], M. Grassi[45], P. Guttridge[8], P. Hakala[46], G. Henri[47], W. Hermsen[38], J. Horak[29], A. Hornstrup[27], J.J.M. in 't Zand[38], J. Isern[5], E. Kalemci[11], G. Kanbach[49],

⋆ marco.feroci@iasf-roma.inaf.it

⋆⋆ luigi.stella@oa-roma.inaf.it

V. Karas[29], D. Kataria[8], T. Kennedy[8],
D. Klochkov[7], W. Kluźniak[9], K. Kokkotas[7],
I. Kreykenbohm[50], J. Krolik[51], L. Kuiper[38],
I. Kuvvetli[27], N. Kylafis[52], J.M. Lattimer[53],
F. Lazzarotto[1], D. Leahy[54], F. Lebrun[33],
D. Lin[14], N. Lund[27], T. Maccarone[31],
J. Malzac[14], M. Marisaldi[12], A. Martindale[42],
M. Mastropietro[1], J. McClintock[55],
I. McHardy[31], M. Mendez[56], S. Mereghetti[57],
M. C. Miller[58], T. Mineo[35], E. Morelli[1],
S. Morsink[59], C. Motch[23], S. Motta[21],
T. Muñoz Darias[21], G. Naletto[18],
V. Neustroev[60], J. Nevalainen[46,77], J. F. Olive[14],
M. Orio[61], M. Orlandini[12], P. Orleanski[62],
F. Ozel[63], L. Pacciani[1,73], S. Paltani[4],
I. Papadakis[52], A. Papitto[34], A. Patruno[3],
A. Pellizzoni[34], V. Petráček[6], J. Petri[23],
P. O. Petrucci[47], B. Phlips[64], L. Picolli[45],
A. Possenti[34], D. Psaltis[63], D. Rambaud[14],
P. Reig[52,76], R. Remillard[65], J. Rodriguez[33],
P. Romano[35], M. Romanova[66], T. Schanz[7],
C. Schmid[50], A. Segreto[35], A. Shearer[67],
A. Smith[8], P. J. Smith[8], P. Soffitta[1],
N. Stergioulas[68], M. Stolarski[62], Z. Stuchlik[69],
A. Tiengo[57], D. Torres[5,79], G. Török[69],
R. Turolla[18], P. Uttley[31], S. Vaughan[42],
S. Vercellone[35], R. Waters[38], A. Watts[3],
R. Wawrzaszek[62], N. Webb[14], J. Wilms[50],
L. Zampieri[37], A. Zezas[52], and J. Ziolkowski[9]

[1] *INAF/IASF, Via del Fosso del Cavaliere 100, I-00133 Roma, Italy*
[2] *INAF/OAR, Via di Frascati 33, I-00040 Monteporzio Catone, Italy*
[3] *Astronomical Institute Anton Pannekoek, University of Amsterdam, The Netherlands*
[4] *ISDC, Geneva University, Switzerland*
[5] *IEEC-CSIC, Spain*
[6] *Czech Technical University, Czech Republic*
[7] *Tuebingen University, Germany*
[8] *MSSL-UCL, United Kingdom*
[9] *N. Copernicus Astronomical Center, Poland*
[10] *Goteborg University, Sweden*
[11] *Sabanci University, Instanbul, Turkey*
[12] *INAF-IASF-Bologna, Italy*
[13] *INAF-Roma, Italy*
[14] *IRAP, France*
[15] *Thales-Alenia, Italy*
[16] *INFN, Bologna, Italy*
[17] *Palermo University, Italy*
[18] *Padova University, Italy*
[19] *LAM - Laboratoire d'Astrophysique de Marseille, France*
[20] *Middle East Technical University, Ankara, Turkey*
[21] *INAF-OA Brera, Italy*
[22] *Politecnico Milano, Italy*
[23] *Observatoire Astronomique de Strasbourg, France*
[24] *INFN, Trieste, Italy*

[26] *INPE, Brazil*
[27] *DTU Space, Denmark*
[28] *Cagliari University, Italy*
[29] *Prague Astron. Institute, Czech Republic*
[30] *Cambridge University , United Kingdom*
[31] *Southampton University, United Kingdom*
[32] *MIT, United States*
[33] *CEA Saclay, France*
[34] *INAF-OA Cagliari, Italy*
[35] *INAF-IASF-Palermo, Italy*
[36] *Racah Institute of Physics, Israel*
[37] *INAF-OA Padova, Italy*
[38] *SRON, Netherlands*
[39] *Durham University, United Kingdom*
[40] *Ferrara University, Italy*
[41] *ISSI Bern, Switzerland*
[42] *Leicester University, United Kingdom*
[43] *SAS/JAXA, Japan*
[44] *ASI, Italy*
[45] *Pavia University, Italy*
[46] *FINCA, Finnish Centre for Astronomy with ESO, Finland*
[47] *Laboratoire Astrophysique de Grenoble, France*
[48] *Helsinki University, Finland*
[49] *MPE, Germany*
[50] *University of Erlangen-Nuremberg , Germany*
[51] *Johns Hopkins University, United States*
[52] *Crete University, Greece*
[53] *State University of New York, United States*
[54] *University of Calgary, Canada*
[55] *Harvard-Smithsonian Center for Astrophysics, United States*
[56] *Groningen University, Netherlands*
[57] *INAF-IASF-Milano, Italy*
[58] *University of Maryland, United States*
[59] *University of Alberta, Canada*
[60] *Oulu University, Finland*
[61] *INAF-OA Torino, Italy*
[62] *Space Research Centre, Warsaw, Poland*
[63] *University of Arizona, United States*
[64] *NRL, Washington, United States*
[65] *MIT, United States*
[66] *Cornell University, United States*
[67] *Galway University, Ireland*
[68] *Aristotle University of Thessaloniki, Greece*
[69] *Silesian University in Opava, Czech Republic*
[70] *NASA/MSFC, United States*
[71] *IESL, Foundation for Research & Technology-Hellas, Heraklion, Greece*
[72] *Institute of Astronomy, University of Zielona Góra, Poland*
[73] *INFN Roma Tor Vergata*
[74] *INAF Headquarters*
[75] *ENEA Frascati*
[76] *FORTH, Crete, Greece*
[77] *Helsinki University, Finland*
[78] *DPNC, Geneva University, Switzerland*
[79] *Institució Catalana de Recerca i Estudis Avançats, Spain*

Received: date / Accepted: date

Marco Feroci for the LOFT team
INAF/IASF, Via del Fosso del Cavaliere 100, I-00133 Roma, Italy
Tel.: +39-06-4993 4099 E-mail: marco.feroci@iasf-roma.inaf.it

Abstract High-time-resolution X-ray observations of compact objects provide direct access to strong-field gravity, to the equation of state of ultra-dense matter and to black hole masses and spins. A 10 m^2-class instrument in combination with good spectral resolution is required to exploit the relevant diagnostics and answer two of the fundamental questions of the European Space Agency (ESA) Cosmic Vision Theme "Matter under extreme conditions", namely: does matter orbiting close to the event horizon follow the predictions of general relativity? What is the equation of state of matter in neutron stars? The Large Observatory For X-ray Timing (LOFT), selected by ESA as one of the four Cosmic Vision M3 candidate missions to undergo an assessment phase, will revolutionise the study of collapsed objects in our galaxy and of the brightest supermassive black holes in active galactic nuclei. Thanks to an innovative design and the development of large-area monolithic silicon drift detectors, the Large Area Detector (LAD) on board LOFT will achieve an effective area of $\sim$12 m^2 (more than an order of magnitude larger than any spaceborne predecessor) in the 2–30 keV range (up to 50 keV in expanded mode), yet still fits a conventional platform and small/medium-class launcher. With this large area and a spectral resolution of $<$260 eV, LOFT will yield unprecedented information on strongly curved spacetimes and matter under extreme conditions of pressure and magnetic field strength.

Keywords Missions, X-ray timing, compact objects, black holes, neutron stars

PACS TBI

1 Introduction

Our knowledge of compact objects derives from the discoveries made with a steady progression of ever larger-area, hence more sensitive, X-ray timing instrumentation, from Uhuru (US, 0.08 m^2, [11]), via satellites such as EXOSAT (ESA, [21]) and Ginga (Japan, [29]) to, most recently, RXTE (US, 0.6 m^2, [27]). The latter instrument, thanks to it having the largest area so far, finally made good on the promise (e.g. [24]) that the process of accretion onto stellar mass collapsed objects should exhibit variability at the millisecond dynamical time scale of the small (few Schwarzschild radii, i.e., kilometres) regions where most of the gravitational potential energy is released. Quasi-periodic oscillations (QPOs) at this time scale were found in the X-ray flux of both neutron stars (kHz QPOs, up to 1250 Hz) and black holes (high frequency QPOs, up to 450 Hz) indicating the action of mechanisms in the strong field region picking out specific frequencies, e.g., orbital and epicyclic motion at specific radii near the marginally stable orbit ($r_{\rm isco} = 6\,GM/c^2$ for a Schwarzschild black hole) as predicted in General Relativity. The long-sought millisecond spins in accreting neutron stars were also finally found, both during thermonuclear bursts (burst oscillations) and in the persistent flux (coherent periodic signals of millisecond pulsars), as were the vibrational responses to cataclysmic events

of some neutron stars themselves (magnetar crust/core oscillations). Relativistically broadened Fe K-lines observed from the accretion disks of both X-ray binaries and active galactic nuclei (AGNs) are thought to arise in the same inner regions of the accretion flow. All these phenomena are direct diagnostics of the motion of matter and the propagation of radiation in very strong gravitational fields: they encode information about the mass, radius and spin of collapsed objects and can probe the properties of ultradense matter and superstrong magnetic fields in neutron stars. Yet tantalizingly, while the relevant signals were identified, due to its still limited sensitivity, RXTE was only able to scratch the surface when it came to actually using these diagnostics to probe strong field gravity and ultradense matter.

LOFT is specifically designed to exploit the diagnostics of very rapid X-ray flux and spectral variability that directly probe the motion of matter down to distances very close to black holes and neutron stars. Its $\sim$20 times larger effective area than RXTE's PCA is crucial in this respect. The key to this breakthrough in effective area resides in the synergy between technologies imported from other fields of scientific research. The crucial characteristic of the LOFT Large Area Detector (LAD) is a mass per unit surface in the range of $\sim$10 kg m^{-2}, enabling a payload with $\sim$15 m^2 geometric area at reasonable weight. The ingredients for a sensitive but lightweight experiment are the large-area Silicon Drift Detectors (SDDs) designed on the heritage of the ALICE experiment at CERN/LHC [30], and a collimator based on lead-glass capillary plates. The drift concept makes the spectroscopic performance of the SDDs weakly dependent on the extent of the collecting surface: large-area ($\sim$70 cm^2) monolithic detectors can be designed, with only 256 read-out anodes (thus low power requirements), but very good spectral performance (FWHM $\sim$260 eV) [32].

An unprecedentedly large throughput ($\sim 3 \times 10^5$ cts s^{-1} from the Crab) is achieved with a segmented detector, making pile-up and dead-time, often worrying or limiting focused experiments, secondary issues. The large detector on LOFT is deployed in space through a mechanism relying on the experience in Synthetic Aperture Radar missions (e.g., the SMOS ESA mission, in orbit since 2009, [2]), where very large panels are deployed in space with high accuracy. This mechanism, combined with the low-weight detector technology, allows the stowing of the LOFT satellite inside the fairing of a Vega launcher to design a small mission in a low-background equatorial LEO ($\sim$600 km). The LOFT scientific payload is completed by a coded-mask Wide Field Monitor (WFM), that uses the same type of detectors, and is in charge of monitoring a large fraction of the sky potentially accessible to LAD, to provide the history and context for the sources observed by LAD and to trigger its pointed observations on their most interesting and extreme states. Its sensitivity and large sky coverage make the WFM also an important resource on its own right.

In this paper we describe the LOFT scientific objectives and expected scientific performance (Sect. 2), mission profile (Sect. 3) and details of the instrumentation and model payload designed to achieve the science objectives (Sect.4).

2 Scientific objectives

2.1 The properties of ultradense matter

One of the key goals of high-energy astrophysics is to determine the equation of state (EOS) of ultradense matter, i.e. the relation between density and pressure at the highest possible densities, where the physics of quarks and quantum chromodynamics (QCD) come into play. At densities exceeding a few times the density of atomic nuclei, exotic states of matter such as Bose condensates or hyperons may appear. At even higher densities a phase transition to strange quark matter may also occur. This high-density/low-temperature region of the QCD phase diagram is inaccessible to terrestrial laboratories and can only be probed astrophysically, where the ultradense matter EOS manifests as a mass-radius (M-R) relation for neutron stars (NS), whose cores contain the densest matter known. Many theoretical EOSs have been proposed through the years, each predicting a different M-R relation for neutron stars. Model EOSs may be classified by the maximum neutron star mass that the EOS can sustain: "soft" EOSs (which produce neutron stars with low central density) have a maximum mass in the 1.5–1.7 solar masses ($M_\odot$) range, whereas "stiff" EOSs can reach up to 2.4–2.5 $M_\odot$ [17]. Recently, a heavy neutron star mass of 1.97 ± 0.04 $M_\odot$ has been measured through accurate timing of a millisecond radio pulsar in a relativistic binary [4], ruling out most soft EOSs and limiting the presence of quark matter in the neutron star core. This is an important step, but the quest for the neutron star EOS is far from settled. We still do not know the radius or maximum mass that a star can support before collapsing into a black hole.

2.1.1 Neutron star mass and radius measurements

Neutron star masses are measured with great precision from binary radio pulsar timing. However, neutron star radius measurements are particularly challenging, and no reliably precise measurements are available to date. Even more challenging is the contemporaneous measurement of M and R, which would allow clear discrimination between EOS models.

Several techniques to estimate M and/or R have been proposed, discussed and used in the past [18]. The best tool to constrain the neutron star EOS is the modelling of coherent X-ray pulsations, that are detected in accretion-powered millisecond X-ray pulsars and during thermonuclear explosions on the surface of many accreting neutron stars ("type I" bursts). The observed pulsed signal is shaped by the brightness pattern on the stellar surface and by gravitational self-lensing by the neutron star's strong gravity, allowing to view more than just the facing hemisphere. This effect alters the amplitude of pulsations generated by rotating "hot spots" on the surface, and it strongly depends on the neutron star M/R ratio. Similarly, the shape of the pulse is affected by the stellar rotational velocity (which depends on the star's radius and hot spot latitude) and by the binary inclination. Modelling the variations

of the pulse shape in different energy bands and at different luminosity levels has been demonstrated effective in constraining mass and radius [19]. Simulations based on RXTE results show that LOFT can achieve ∼5% precision in radius measurement with such observations. Effective discrimination between different families of EOSs will be possible only with such a relative precision.

In ∼25 neutron stars, coherent oscillations at frequencies of up to 620 Hz are also observed during type I X-ray bursts, which are mostly the result of thermally unstable helium ignition in the accreted envelope of a neutron star. This generates a thermonuclear explosion that is observed as an X-ray burst with a rapid rise (∼1 s) followed by a slower decay (∼10–100 s). X-ray pulsations can be measured with sufficient precision during the burst rise (i.e. when the X-ray emitting area grows) by a detector with very large effective area. Simulations show that with LOFT we can achieve an error of less than 5% (90% c.l.) on both M and R, firmly constraining the EOS.

In the X-ray spectra of two photospheric radius expansion bursts observed with the RXTE satellite, despite the low spectral resolution, strong absorption features were detected during the early expansion phase with a timescale of ∼1 s [12]. These features are predicted due to the presence of ashes of nuclear burning in the photosphere. The changing edge energy during the burst precluded a measurement of the gravitational redshift and the low resolution an unambiguous identification of nickel as the element. Future measurements with larger effective areas and moderately higher spectral resolution, like provided with LOFT/LAD, will determine the redshift at the neutron star surface.

Fast rotation of compact stars is sensitive to the stellar mass and to the EOS, constraining the star spin against centrifugal break-up. The fastest known neutron star spin (716 Hz, and, if confirmed, 1122 Hz) already rules out an entire class of models predicting large, low-mass neutron stars. This search in X-rays has no known biases against the detection of very high spin rates (unlike radio pulsation searches) and if carried out with a very large area as LOFT's will achieve very high sensitivities: a pulsed fraction of 0.8% and 0.07% will be detected at $5\,\sigma$ with a 100 s observation of a 100 mCrab source and Sco X-1, respectively. The observed lack of extremely high spin frequencies (>800 Hz) in the most rapidly accreting neutron stars also suggests that their accretion torques might be balanced by gravitational wave emission torques. LOFT will provide a complete census of periods in X-ray binaries. Moreover a precise knowledge of the spin periods of fast spinning neutron stars can greatly increase the sensitivity of the searches for their gravitational wave signals with interferometers such as Advanced Virgo/LIGO.

2.1.2 Neutron star crust properties

In 2004, the magnetar SGR 1806-20 emitted the most powerful flare ever recorded, with a fluence of several 10^{47} ergs (a.k.a. giant flare), affecting even the Earth's ionosphere. QPOs (∼10% rms amplitude) in the 18–1800 Hz range were detected in the X-ray band during the decaying tail of the flare [13]. Similar results were obtained for SGR 1900+14 by re-analyzing the X-ray archival

data of its 1998 giant flare [26]. Detection of signals at similar frequencies in the giant flares from two different magnetars implies that the same process is operating in both objects. Powering the rare giant flares requires a catastrophic reconfiguration of the magnetic field and likely implies large-scale crust fracturing (i.e. starquakes). This in turn should excite coupled crust-core ("seismic") oscillations observed in the X-rays as QPOs. Different types of these global seismic oscillation (GSOs) are possible, torsional magneto-elastic modes in particular are expected to give rise to the observed oscillations. The harmonics which are excited depend on the size, shape and speed of the fracture. The observed mode frequencies depend on the neutron star mass and radius, crustal composition, core superconductor state and magnetic field strength and configuration. The identification of the GSOs modes discovered in the two giant flares remains a subject of active theoretical debate. At present it seems possible to explain them in terms of magnetic-elastic modes dominated either by the magnetic field or by the crust, depending on the state of the core superconductor.

Giant flares are rare and the chances that one of them occurs during the operational lifetime of LOFT are fairly low (30%). On the other hand, theory tells us that GSOs should be excited also during the much more frequent (tens during active states) but less energetic events called intermediate flares (duration 1–60 s, fluence up to 10^{43} ergs). LOFT, thanks to its large area and monitoring capabilities, will be able to detect and study in depth magnetar QPOs during intermediate flares. This will be done on bright and hard serendipitous events shining in the experiment from directions outside the field of view (in this case the LAD response will be mostly above ∼20–30 keV, by using the extended energy range, where the collimator opacity decreases) or by direct pointing of magnetars in their burst active state, following a trigger by the WFM (in which case the events will be covered with the whole effective area of the LAD down to energies of 2 keV). Studying these events with LOFT's exceptionally high throughput will detect much weaker magnetar QPOs than observed so far, thus probing the interiors of neutron stars in a similar manner to helioseismology. A 500 Crab intermediate flare shining at 30° offset angle in the LAD collimators would allow the detection of magnetar QPOs with amplitudes as low as 5% and 0.7%, respectively, for a flare duration of 1 s and 60 s (Fig. 1).

Searches for seismic oscillations can be also carried out in glitches observed in magnetars as well as in rotation-powered radio pulsars. Glitches are thought to originate from a sudden unpinning of angular momentum vortices in the neutron star crustal superfluid. The recovery from a glitch contains information on the neutron star interior and in particular on the coupling between crust and core. Differences among the behaviour of radio pulsars and magnetars can lead to the discovery of systematic structural differences between the two types of neutron stars.

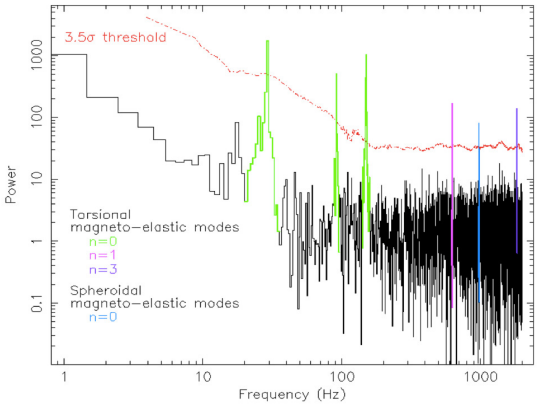

Fig. 1 Frequencies expected in the power spectrum of a magnetar intermediate flare as seen by LOFT.

2.2 Strong gravity and the mass and spin of black holes

Most of the power generated by accretion onto neutron stars and black holes is released deep in the gravitational potential wells of these objects, where the matter flowing inwards moves at a sizable fraction of the speed of light. Observation of the motion of matter in the innermost regions of accretion disks contains unique information on the properties of the strongly curved spacetime near neutron stars and black holes, and on the compact object's mass, spin and size. Over the last two decades powerful diagnostics of the innermost disk regions have been discovered: among those based on timing measurements are the QPOs in the flux of a number of X-ray binary systems (and until now one active galactic nucleus) which occur at the dynamical time scale of the innermost disk regions and hence are associated to the fundamental frequencies of matter motion in strong field gravity. The Fe K_α emission lines which are observed in many accreting collapsed objects, from neutron stars to supermassive black holes in AGNs, are powerful spectral diagnostics that form a second, independent probe of the same strong field gravity regions.

The exploitation of these diagnostics has so far been hampered by insufficient throughput and/or energy range and resolution of the instrumentation. For instance, in about 20 neutron star binary systems, a diverse QPO phenomenology was observed with RXTE. At high frequencies (200–1200 Hz), pairs of signals are observed, whose frequencies vary on timescales as short as hundreds of seconds. These QPOs can be strong, but their intensity is highly variable. Averaging these signals over thousands of seconds, sometimes days in order to detect them, has until now prevented the exploitation of the full potential of this diagnostic. A somewhat similar phenomenology is observed in several black holes, but their QPOs are weaker and even more difficult to detect, especially at high frequencies. The current indication is that the frequencies of these high frequency QPOs are rather stable for each system and

anti-correlate with the black-hole mass. In a few cases where two frequencies can be identified, they appear to be at special ratios of 2:3 and 3:5. These features have been detected rarely and only in a specific state when sources are bright, nearly certainly because only then they peak up to levels detectable with present instruments [31].

2.2.1 Neutron star and stellar mass black hole

The origin of QPOs in neutrons stars and black holes is still open to different interpretations, but all viable explanations include a hydrodynamical flow in which the fundamental frequencies of motion (azimuthal, epicyclic) in the strong gravitational field near these objects dominate the motion. In this region, GR effects are important: for instance there is no post-Newtonian treatment that could approximate the behaviour of the radial epicyclic frequency in this regime. The magnitude of general relativistic effects is thus not an issue. It is crucial instead to make sure that the QPO diagnostics are interpreted correctly. The major leap in the effective area that LOFT provides will permit for the first time to exploit new, qualitatively different techniques for extracting physical information from the QPOs. In the following we describe a few examples of this.

The relative "simplicity" of the space-time around black holes (cleared of the complications of solid surface, magnetosphere and internal mass distribution effects on the external spacetime that affect neutron stars) makes the theoretical modeling relatively straightforward, thus the observational tests particularly relevant and conclusive. Methods have been devised to test the models through detailed high signal to noise observations. For instance, in the parametric epicyclic resonance model two of the oscillation modes are associated with a resonance of the relativistic radial and vertical epicyclic frequencies [1]; in the relativistic precession model instead, the highest frequency signal is identified with the azimuthal frequency of motion, while two of the modes arise from relativistic nodal and periastron precession (whose frequency is related also to the epicyclic frequencies [25]). By studying the QPO behaviour over a range of source intensities LOFT will afford to remove the current degeneracy in the interpretation of the oscillation. Once the ambiguity in the interpretation of the QPO phenomena is resolved, the frequencies of the QPO themselves, which LOFT measures with exquisite precision, will immediately provide access to yet unobserved general relativistic effects such as Lense-Thirring and strong field periastron precession, or the unique behaviour of the epicyclic frequencies near a black hole. As these frequencies embody also information on the black hole mass and spin, these can thus be derived or, at least, tightly constrained.

LOFT will enable the study of the QPO signals in time (as opposed to Fourier) domain; in particular, low frequency QPOs will be studied in individual pulses and kHz QPO within their coherence timescale. (The latter requires a minimum effective area of $\sim$10 m^2). Time-domain studies will open a new dimension in the exploitation of QPOs: it will permit to directly observe the

decoherence process and recurrence of these signals, measure waveforms and their energy dependence, perform phase-resolved spectroscopy, and compare these direct diagnostics of what is going on at the relevant (for the high frequency QPOs: dynamical) timescales with numerical work predicting these behaviours of the accretion flow. This will be crucial to decide whether QPOs originate from, e.g., orbiting hot spots and disk vibration or warping modes.

In nearly all cases discussed above, additional information will be derived from the time-averaged Fe K_α fluorescence line profile. As is well known, relativistic effects such as gravitational redshift, light-bending, framedragging, and Doppler shifts distort the iron line shape into a characteristic broad shape. Measurements of the line profile then translate into measurements of the innermost radius of the disk (in natural units of $r_g = GM/c^2$), the inclination and emissivity law of the disk. Through the effects of frame dragging on the innermost stable orbit, this leads to the determination of the spin of the black hole. This spectroscopic measurement of the matter motions near the central object can be combined with timing measurements to derive compact object mass and orbital radii. The energy resolution and large area of LOFT will allow measurements of unprecedented quality for this relativistically broadened iron line and its variations.

We illustrate here an example of the potential of the combined exploitation of flux and spectral variability with LOFT, under the hypothesis that the low frequency QPO originate from the nodal precession of the innermost disk region as envisaged in some QPO models. The varying inclination angle caused by precession will induce a characteristic variation in the width and profile of the Fe K-line produced by the innermost disk region. Fig. 2 shows the result of a simulation in which the inner disk ring of the accretion disk undergoes a 30 Hz nodal precession with a 5 degrees tilt angle relative to the rest of the disk; the LAD will reveal the precession of the inner disk with very high significance.

2.2.2 Supermassive black holes

Bright AGNs provide an additional and somewhat complementary opportunity to study strong field gravity. Though their flux at the Earth is typically 100–1000 times lower than that of accreting black holes in galactic binaries, their dynamical timescales (which scale with the mass) are $\sim 10^6$ times longer. The result is that some 10^3 times more photons are received at the Earth per dynamical timescale from bright AGNs than from X-ray binaries. Therefore bright AGN provide a parallel channel for investigating individual realizations of very short term phenomena, such as the motion of a single spot in the disk or the response of the Fe-line disk emissivity to flares from the illuminating source.

As in X-ray binaries, the relativistic broad Fe-line profile that is seen in the X-ray spectrum of a number of AGNs (about 70% of bright Seyfert 1), provides a powerful tool to probe the accretion flow in a region where the motion is determined by GR [7, 16]. Evidence for spinning supermassive black

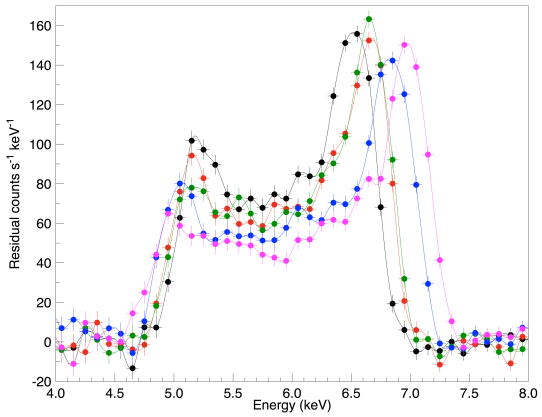

Fig. 2 Contribution to the Fe line emission of a small ring (9–10 r_g) of matter undergoing nodal (Lense-Thirring) precession around a neutron star. The different line profiles are computed for different phase of the precessional motion; the tilt angle relative to the disk is 5° around the system inclination (26°). The simulation here is representative of the case of the 300 mCrab neutron star binary GX 349+2. The figure shows the contribution from the ring emission, after removal of the continuum and steady Fe-line components.

holes has been found in several cases. LOFT will determine with very high signal to noise and accurate continuum subtraction the profile of AGN Fe K-lines, thanks to its sensitivity and broad energy range. The instrumental and cosmic background in the LAD will permit to study AGNs in this context down to flux level of ∼1 mCrab, with signal to noise ratios of about 500 in 10^4 s exposure. With a 10^3 s exposure, LOFT will collect more than 5×10^5 counts in 2–30 keV for a 3 mCrab AGN: that will provide a high enough S/N to determine accurately the Fe line profile and measure the inner radius of the disk down to the marginally stable orbit and from this derive the spin of the BH.

Moreover, LOFT's very high throughput will permit to investigate the line response to flares and reveal the orbital motion of individual blobs illuminated by the central source through the moving features that they induce in the line profile [5]. These "reverberations" will provide the physical unit for the emitting radius that is required to measure also the black hole mass in addition to the spin. An example of the expected performance of LOFT on this subject is shown in Fig. 3.

2.3 Additional Science Objectives

In addition to the main science goals outlined above, LOFT will very successfully exploit the physical information contained in the flux and spectral variability of many different classes of sources to address a number of open astrophysical problems. The longer timescale variability will be explored by the WFM, singling out specific source activities and/or spectral states (e.g.

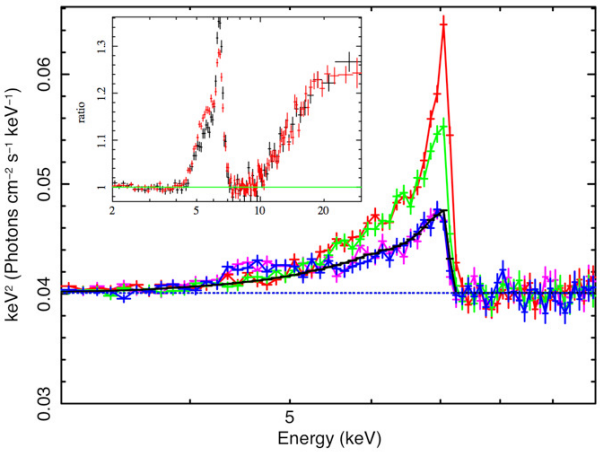

Fig. 3 Simulated LOFT/LAD spectra of a 3 mCrab (2–10 keV) AGN. The lower plot shows the broad relativistic Fe line produced in the innermost region of the accretion disc extending down to the marginally stable for an almost-maximally rotating black hole ($a = 0.99$) with mass of 3.6×10^6 $M_\odot$, viewed at an inclination of 45 deg. The plot shows the variable Fe K feature produced by an orbiting spot at $r = 10\,GM/c^2$ on the disk's surface that is illumination by a flare. The orbital period is 4 ks and the total exposure is 16 ks. LOFT/LAD will track the line variation on 1 ks time scale, thus allowing a determination of the orbital period through measurements at four different orbital phases over four cycles. The inset shows two 10 ks spectra from simulated high (6 mCrab in 2–10 keV) and low (2 mCrab) flux states LOFT/LAD observations of MCG-6-30-15. Thanks to the wide energy band and the large effective area above 10 keV, the variation of the reflection hump can be measured with 2% accuracy.

those of accreting millisecond transient pulsars) amongst many hundreds of monitored sources. Clearly the WFM will be essential to trigger and carry the LAD observations required to achieve LOFT's main science objectives. In the following we briefly outline some of additional science themes to which LOFT will give great contributions.

X-ray binaries are the brightest sources of the X-ray sky. LOFT will be able to detect periodicities of unprecedented small amplitude and measure their phase and period evolution to high accuracy. By means of the study of periodic signals, several issues could be investigated:

- the physics and geometry of accretion onto magnetic white dwarfs and neutron stars;
- the torques responsible for their secular spin up and down and the instabilities giving rise to glitches;
- evidence for the long-sought photon bubble instability in the accretion column above magnetic neutron stars;
- intermittent millisecond pulsations in accreting X-ray binaries.

Millisecond radio pulsars also emit in the X-ray band. A large number of γ-ray sources have been discovered with Fermi, that are suspected to be fast

rotation powered pulsars. However, many of these are in regions of the Galaxy behind large foreground columns of ionized gas and dust, implying that neither radio, nor soft X-ray followup will be able to confirm their nature; however, a large area hard X-ray timing mission like LOFT should be able to detect the pulsations from many such objects.

The mechanism for the launching of jets is still poorly understood. The WFM's excellent sensitivity will allow us to trigger early on new X-ray transients, and hence to use the LAD for multi-wavelength campaigns in conjunction with optical and IR instruments with sub-second time resolution (e.g. ISAAC on the VLT, and SALTICAM on SALT). Cross-correlations between X-rays and optical/IR can be used to estimate jet speeds even in cases where the spatial scale of the jets are too small to be resolved spatially. By being able to make these measurements over a wide range of luminosities for the same sources, it will be possible to determine relations between jet speeds and luminosities and accretion states.

WFM's large instantaneous field of view is another important advantage of LOFT over past soft X-ray all-sky instruments. This gives LOFT an unprecedented capability for detecting rare, short-lived, bright sources, such as Gamma Ray Bursts, X-ray flashes, X-ray transients of all classes , and for obtaining high cadence monitoring of moderately bright sources. One of the RXTE highlights was the monitoring of many active galactic nuclei using pointed observations that allowed to demonstrate that many of these systems had power spectral breaks similar to those seen in X-ray binaries. Similar monitoring, with much better sampling, can be done on all similarly bright AGNs with LOFT/WFM. Pointed observations with the LOFT/LAD will be able to detect short term variations of $\sim$1–3 mCrab AGNs with unprecedented sensitivity. Hard X-ray monitoring of flaring blazars is especially important, since there is a strong correlation between hard X-ray activity and high-energy gamma-ray activity. LOFT's WFM can be used to trigger ground-based Cherenkov telescopes, and comparisons of the synchrotron peak in the X-rays with the Compton peak in the gamma-rays can be used to provide constraints on the cosmic infrared background.

3 Mission profile

The scientific requirements of the LOFT payload as derived by the science objectives are summarized in Table 1. The key system requirements of the LOFT mission to meet such scientific requirements are the accommodation of the structure hosting the Large Area Detector (LAD), having a $\sim$20 m^2 surface area, and the powering of such a large detector ensemble. A preliminary evaluation by Thales Alenia Space Italy (TAS-I), on behalf of INAF, has identified a mission concept combining such a large structure with a standard service module. By means of deployment mechanism technologies derived from

LAD

Parameter	Requirement	Goal
Energy range	2–30 keV (nominal) 2–50 keV (expanded)	1–40 keV (nominal) 1–60 keV (expanded)
Eff. area	12.0 m^2 (2–10 keV) 1.3 m^2 (@30 keV)	15 m^2 (2–10 keV) 2.5 m^2 (@30 keV)
ΔE (FWHM, @6 keV)	<260 eV	<180 eV
FoV (FWHM)	<60 arcmin	<30 arcmin
Time res.	10 μs	5 μs
Dead time	<0.5% (@1 Crab)	< 0.1% (@1 Crab)
Background flux	<10 mCrab	< 5 mCrab
Max. src flux (steady)	>0.3 Crab	>10 Crab
Max. src flux (peak)	>15 Crab	>100 Crab

WFM

Parameter	Requirement	Goal
Energy range	2–50 keV	1–50 keV
ΔE (FWHM)	<300 eV	<200 eV
FoV (FWHM)	>3 steradian	>4 steradian
Ang. res.	5 arcmin	3 arcmin
PSLA	1 arcmin	0.5 arcmin
Sens. (5σ, 50 ks)	2 mCrab	1 mCrab
Sens. (5σ, 1 s)	0.5 Crab	0.2 Crab

Table 1 Scientific requirements for the LOFT LAD and WFM instruments.

SAR missions, like the ESA's SMOS [22], the satellite can be stowed within the launcher fairing volume of a Vega, the small ESA launcher. Considering a launch into a Low Equatorial Orbit (LEO, ∼600 km) and the estimated mass of the flight segment, the Vega launcher still provides a fairly large mass margin.

Although LOFT/LAD observations are largely source-dominated in most cases, the science objectives related to the AGNs are very sensitive to the issue of the background minimization and stability, highly benefiting from the choice of a circular, equatorial (<5° inclination) LEO. The latter will be also very effective in minimizing the long-term radiation effects on the detectors.

LOFT has a higher data throughput compared to previous X-ray missions. We envisage a telemetry downlink to the Kourou (ESA) and also to the Malindi (ASI) equatorial ground stations. In this scenario each ground station will have a ∼10-min contact every ∼100-min orbit. Kourou will be used for both telecommand uplink and telemetry downlink. Malindi for telemetry downlink only. The maximum rate available to the scientific telemetry (orbit average) in this configuration is ∼700 kbps.

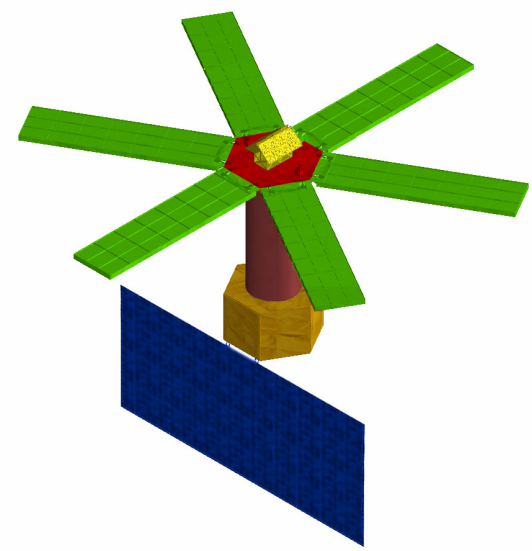

Fig. 4 Conceptual scheme of the LOFT satellite. (green) Large Area Detector, (yellow) Wide Field Monitor, (red) Optical Bench, (purple) Structural Tower, (gold) Bus and (blue) Solar Array.

The LOFT mission is expected to operate in three-axes stabilized pointing mode. The slew rate capability is estimated in about 4°/minute. The solar panel array is fixed, and the Sun aspect angle constraint is set at ±20°. An orbital simulation has been performed considering a launch in 2022 (solar minimum period) and ballistic coefficient based on the nominal satellite attitude. The simulation shows an orbital decay of ∼20 km in a period of 5 years. Based on these preliminary evaluations it is possible to assert the feasibility of LOFT mission as a small-medium class mission in LEO equatorial orbit, with a Vega launch vehicle.

4 Model Payload

To meet the scientific requirements summarized in Table 1 and to achieve the science objectives summarized in Sect. 2, the LOFT scientific payload is composed of two instruments: the Large Area Detector (LAD) and the Wide Field Monitor (WFM). Both experiments rely on the technology of the large-area Silicon Drift Detectors (SDDs), although with application-specific detector design details. In Fig. 4 the different components of the LOFT satellite are identified: the LAD is composed of 6 Detector Panels (DPs) deploying from an optical bench, hosting the WFM at its center, observing a sky region including the field of view of the LAD.

4.1 The Large Area Detector (LAD)

The LAD is a collimated experiment, conceptually similar to its predecessors (e.g. RXTE/PCA, [14]). The development of a 10 m^2-class experiment is now made possible by the recent advancements in the field of large-area silicon detectors - able to time tag a X-ray photon with an accuracy <10 μs and an energy resolution of ∼250 eV FWHM - and capillary-plate X-ray collimators. The relevant feature of the LOFT design is the low mass and power per unit area enabled by these two elements. In this respect, the key properties of the Si drift detectors (see e.g. [10]) are their capability to read-out a large photon collecting area with a small set of low-capacitance (thus low-noise) anodes and their very small weight (∼1 kg m^{-2}).

4.1.1 The detector

The primary enabling technology for the LAD is the large-area Silicon Drift Detectors (SDDs) based on the heritage of the detectors developed for the Inner Tracking System (ITS) in the ALICE experiment of the Large Hadron Collider (LHC) at CERN, by INFN Trieste, Italy - in co-operation with Canberra Inc. [23, 30].

The LAD detector design is indeed an optimization of the ALICE detector: 6-inch, 450 μm thick wafers will be used to produce 76 cm^2 monolithic SDDs (108.52 mm×70.00 mm active area). The anode pitch is increased to 854 μm (corresponding to an elemental area of 0.854 mm×35 mm = 0.299 cm^2) to reduce the power consumption and improve the low-energy response. The Si tile is electrically divided in two halves, with 2 series of 128 read-out anodes at two edges and the highest voltage along its symmetry axis. The drift length is 35 mm. A drift field of 370 V/cm (1300 V maximum voltage), gives a maximum drift time of ∼5 μs [15] at room temperature, constituting the detector contribution to the uncertainty in the determination of the time of arrival of the photon. Indeed, with the above electric field, the charge will typically distribute over 1 (40% of events) or 2 (59% of events) anodes, rarely on 3 (1% of counts). The segmentation of the detector makes the dead time and pile-up risks negligible (see below), a crucial property for a timing experiment.

In Fig. 5 we show examples of energy spectra of a ^{55}Fe source (with lines at 5.9 and 6.5 keV) obtained at 20°C, by instrumenting a spare ALICE SDD with discrete electronics. The energy resolution is ∼300 eV FWHM on single-anode events and the low energy discrimination threshold is below 0.6 keV (see [32] for details).

The detectors as optimized for the LOFT application will achieve even better performance. In fact, the current performance of the prototype breadboard at room temperature (see [32]) will be improved by the use of an integrated read-out electronics that will largely reduce the parasitic capacitance, and by the instrument operation at low temperature, decreasing the leakage current by more than an order of magnitude, even in the larger thickness and pitch

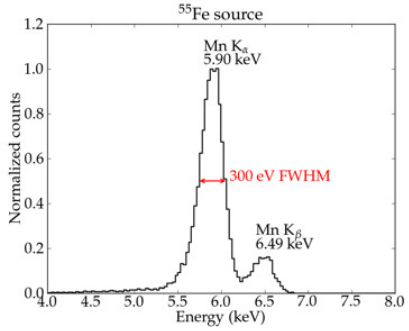

Fig. 5 Energy spectra measured using a spare ALICE detector equipped with discrete read-out electronics, at room temperature. The FWHM energy resolution was measured as ∼300 eV at 5.9 keV.

configuration of LOFT, as well as with the expected level of radiation damage in orbit.

4.1.2 The collimator

The other key element of the LOFT payload innovative design is the capillary-plate X-ray collimator (although collimators based on the same technology were already used in the Medium Energy experiment onboard EXOSAT, [28]). This is based on the technology of micro-channel plates. A multi-pore, ∼mm thin sheet of lead-glass is able to absorb soft X-rays coming from outside its aperture holes. Standard collimators can be procured off-the-shelf with a 50% lead content in the glass, offering a significant stopping power to soft X-rays. We studied the angular response to different photon energies with GEANT Monte Carlo simulations and the results demonstrate an effective shielding up to ∼40 keV, above the energy range of LOFT. Photons with higher energy passing through will be detected with low efficiency by the thin Si detector and will be anyway discriminated by their energy deposition, except for the Compton interactions that will contribute to the residual instrumental background. A noticeable property of these devices is their very low weight. The LOFT baseline is a 2 mm thick plate, with inner hole diameter of 25 μm and pitch of 28 μm (field of view 43 arcmin FWHM, OAR=80%): the net weight is about 3 kg m^{-2} enabling large areas at reasonable mass and costs.

4.1.3 The Front-End and Back-End Electronics

The requirements of fine pitch, small parasitic capacitance, low-power consumption and the need for tiling imply a high-density read-out system, based on ASICs (Application Specific Integrated Circuits). The low capacitance of each anode allows us to reach ultra low noise levels and short optimum signal processing time ($\simeq$1 μs). The specifications for the baseline LOFT ASIC, developed by Polytechnic of Milan and University of Pavia include: an input

range of 0.5–100 keV (135–27000 e^-); a noise $\leq$ 20 e^-_{rms}; 12 bit ADC resolution; a time tagging accuracy of an event to better than 1 μs and a power consumption <540 μW/channel (all inclusive).

The event processing time in the ASIC drives the dead time of the system. Even in the worst case of an event involving 3 anodes (less than 1% of the cases), the corresponding detector area being 0.9 cm^2, the SDD read-out time <10 μs makes the pile-up probability negligible ($<10^{-4}$ for a source with a flux lower than 5 Crab). Based on the ASIC architecture, nearly simultaneous triggers on different channels will be processed independently. The source count rate during the Crab observation will then cause a dead-time <0.03%.

A back-end electronics (BEE) is in charge of interfacing the front-end electronics (FEE) with the Payload Data Handling Unit (PDHU). It is organized hierarchically, with one Module Back-End Electronics (MBEE) for each of the 21 Modules in a Detector Panel (DP), connected to one Panel Back-End Electronics (PBEE) for each of the 6 DPs. The full LAD will then have 126 MBEEs and 6 PBEEs. The tasks of the BEE will include: power supply, post-regulation and filtering; interfacing the digital output of the 16 FEEs (each one including 8 ASICs) of each Module, as well as the PDHU; event trigger filtering and time tagging; pedestal subtraction; cluster identification and validation.

4.1.4 The LAD Detector Panel organization

The basic LAD detection element is composed of SDD, FEE and collimator. The assembly philosophy envisages a hierarchical approach: Detector, Module, Panel, LAD Assembly. To provide an efficient tiling, with the required mechanical stiffness and alignment accuracy, the procedure for the Module integration includes a reference frame where the 16 collimators in a Module can be accurately integrated with the detector and the FEE (Fig. 6). The latter is composed of a thin printed circuit board, designed to host the SDDs on one side and the ASIC and electronics component on the opposite side, with pass-throughs for electrical connections. The power lines to the voltage divider (HV and MV) are brought from the back (p-side) to the front (n-side) pads of the Si tile by a wrap-around flex cable, similar to that designed for the ALICE experiment [20].

The SDDs are sensitive to visible/UV light, which causes an increase in the leakage current. To prevent this, each detector will be equipped with a multilayer blanket, operating both as a light and thermal shield. We selected 1 μm thick Polymide film coated with 0.08 μm Aluminum. This choice will ensure an optical transmission below 10^{-6}, and a soft X-ray transmission greater than 90% at 2 keV.

The back side of the Module (Fig. 6, center) will also host the mechanical interface to the Module Back-End Electronics (MBEE), as well as a shield to stop photons from the cosmic X-ray background. The surface of the MBEE will also be designed as a radiator. The power generation in a Module is evenly shared between MBEE and detectors: a larger detector radiator will favor a lower temperature on the SDDs and ASICs, improving the performance, while

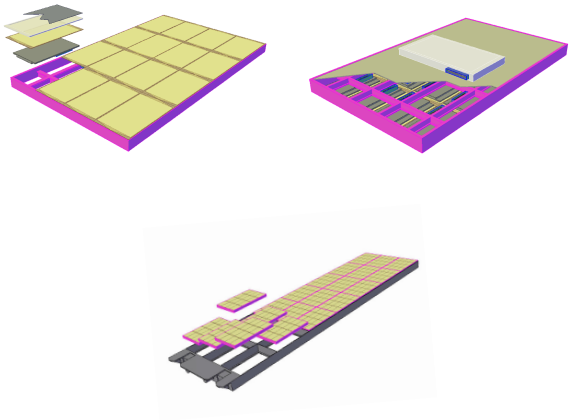

Fig. 6 *Left:* One LOFT Module (top view). *Right:* One LOFT Module (bottom view). *Below:* A LOFT Detector Panel.

keeping the rest of the electronics at moderate cooling. A set of 21 Modules will be integrated into a Detector Panel (DP, Fig. 6). This is a mechanical frame providing mechanical support and alignment interfaces for the individual Modules, for the Panel Back-End Electronics (PBEE) box and enabling the electrical connection and routing between the 21 MBEEs and the single PBEE in each DP. The DP will have mechanical and alignment interfaces with the LAD deployment mechanism.

The LAD deployment mechanism will allow the LAD to be launched in a stowed position that fits within the Vega fairing. The basic mechanism draws on the heritage of Synthetic Aperture Radar (SAR) panel deployment systems. This type of mechanisms guarantees accuracy and repeatability in the panel deployment in the sub-arcmin range (e.g., [2]). The preliminary LOFT satellite configuration consists of 6 DPs, connected to the satellite optical bench by hinges. The mechanisms will provide the deployment with a pure mechanical control and motorization.

The LAD experiment has a favorable structure for temperature control, due to the uniform power generation over the DPs, that can be used in the thermal balance with irradiation for a passive thermal control. Indeed, a preliminary thermal analysis shows that the LOFT detector panels are expected to operate at temperatures between -30°C and 0°C, depending on the Sun aspect angle and the thermal design, with a short-term (e.g., orbital) variation of less than ∼3°C. A design optimization will be performed to achieve a low and stable operating temperature, needed for an optimal detector and FEE performance.

4.1.5 Mass, Power, and Telemetry budgets

Based on the preliminary design described in the previous sections, we evaluated detailed mass and power budgets. Our evaluation shows an overall satel-

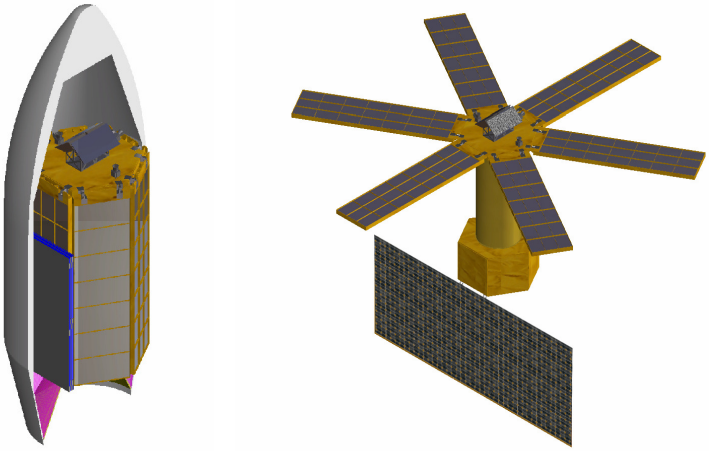

Fig. 7 The LOFT satellite inside the Vega launcher (left) and after the deployment of the LAD and of the solar array (right).

lite mass of ∼1800 kg, including both sub-system and system level margins, with approximately 60% allocated to the payload. The power budget was also computed on the basis of detailed subsystem estimation. The total power required by the satellite, including all the subsystem and system margins, is ∼1800 W, compliant with the available power generated by a solar panel array that can fit the satellite and launch constraints.

The LAD telemetry budget is estimated under the following assumptions: *i*. default event-by-event data transmission, *ii*. individual event info: ∼60 eV energy bin below 30 keV, ∼2 keV in 30–50 keV (expanded range), 2 μs time resolution and *iii*. absolute time event every 100 ms, and differential event time tagging. In estimating the telemetry budget, we assume a source with intensity 500 mCrab permanently in the field of view (this flux threshold includes >95% of the known X-ray sources with flux above 1 mCrab, [6]). The overall LAD telemetry budget is ∼600 kbps, through a lossless compression algorithm (factor of ∼3-4). A mass memory on the PDHU will allow the temporary storage of excess telemetry. Some of the key science targets (∼10 persistent sources and some bright X-ray transients) will exceed the above flux threshold assumption. In these cases we will employ a flexible set of data modes, as was done with the Event Data System (EDS) on RXTE. These modes allow the time and energy binning to be optimized for the science goals within the available telemetry budget.

4.1.6 The LAD effective area

The preliminary design described in the previous sections allows to obtain an effective area for the LAD as shown in Fig. 8, as a function of energy. In

the same plot the effective area of timing experiments onboard previous and planned missions is shown for comparison. The plot is shown in both log-log and log-lin scale, as the sensitivity for the QPOs scales linearly with the count rate, that is with the effective area: the linear vertical scale allows to appreciate the breakthrough offered by LOFT in this field.

The energy dependence is driven by the detector properties. The effective area peaks at a value of $\sim$12 m^2 in $\sim$5-10 keV. The factor primarily affecting the resulting peak effective area with respect to the $\sim$15 m^2 geometric area is the open area ratio of the collimator.

The low energy decrease is due to the passive materials intervening in the detector field of view (including both the detector passive layers and electrodes, as well as the optical-thermal blanket). In the energy range between 1 and 2 keV an effective area as large as $\sim$5 m^2 is still available in principle. However, the current baseline for the low energy threshold is set at 2 keV: a lower energy threshold is a goal and it is currently being investigated. At high energies the decrease of the effective area is due to the decreasing quantum efficiency of the 450 μm thick silicon. However, a noticeable value of $\sim$1.3 m^2 for the effective area is still available at 30 keV, significantly larger than any other timing experiment (Fig. 8). Improvements at higher energies require thicker detectors, that are currently under study.

4.2 The Wide Field Monitor (WFM)

The scientific requirements of the WFM are reported in Tab. 1. The WFM is composed of 4 coded mask cameras for a total geometric area of 1600 cm^2, hosted on the top of the LAD tower. It is designed on the heritage of the SuperAGILE experiment [9], successfully operating in orbit since 2007 (e.g., [8]). The latter demonstrated the feasibility of a compact, large-area, light and low-power, arc minute resolution X-ray imager, with steradian-wide field of view. The LOFT WFM applies the same concept, with improvements provided by the superior performance of the large area SDDs (similar to those in the LAD, but with a finer anode pitch) in place of the silicon microstrips. The different detectors and their configuration allow the LOFT/WFM to operate down to much lower energies (2 keV).

By using the large area SDDs, with a position resolution $<$100 μm, a coded mask at $\sim$150 mm provides an angular resolution $<$5 arc min. The coded mask imaging is the most effective technique to observe simultaneously steradian-wide sky regions with arc min angular resolution. In contrast to their use in the LAD, in the WFM the position resolution of the SDD is a key issue. For this reason the baseline WFM SDDs have a $\leq$300 μm anode pitch. Using the lab tests of the ALICE spare detector (see Sect. 4.1.1) and an accurate Monte Carlo simulation of the detector physics, we estimated a position resolution better than 60 μm FWHM along the anodes and $\sim$8 mm FWHM along the drift channel [3]. The latter exploits the electron cloud diffusion during the

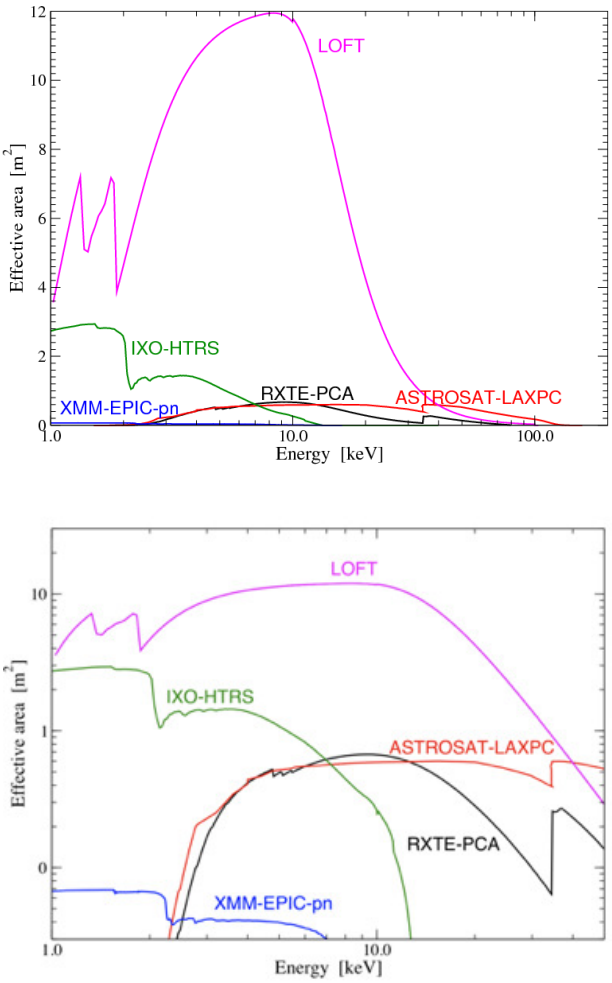

Fig. 8 LAD effective area (vs. energy) plotted in both linear and logarithmic scale, as compared to that of other satellites for X-ray astronomy.

drift that makes the charge distribution over contiguous anodes dependent on the drift distance.

Due to the coarse detector position resolution along the drift direction, we conservatively consider the WFM camera as 1-D and we require 2 orthogonal cameras to image the same sky region at any time for fine source positioning in 2-D. This is the same technique used in SuperAGILE, RossiXTE/ASM or HETE/WFM. However, in the LOFT/WFM the coarse position resolution in the drift direction in each camera reduces considerably the source confusion in crowded fields (e.g., Galactic Center). The design of a single WFM camera (Fig. 9) consists of a tiled 20 cm×20 cm detector plane (6 large-area 450 μm

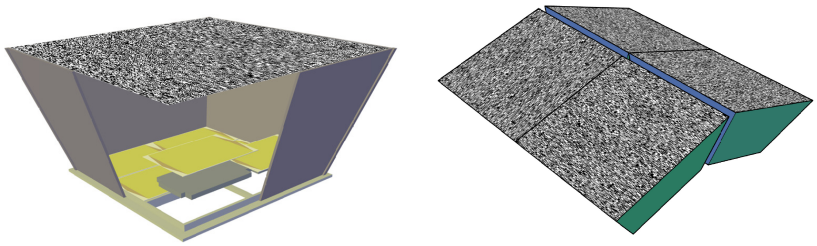

Fig. 9 The Wide Field Monitor.

thick SDDs), an asymmetric 2-D coded mask and a collimator. The SDD readout employs the same ASICs as the LAD, with a proper design customization to the finer pitch. A light collimator (e.g., 1 mm thick carbon fibre, covered with a 150 μm tungsten sheet) effectively shields the X-ray photons from the diffuse X-ray background (the main background source, as charged particles are efficiently rejected by the amplitude discrimination) up to energies above 60 keV. The 150 μm thick tungsten mask (Fig. 9) has a pitch of $\sim$250 μm and $\sim$16 mm in the two directions, respectively. The mask size is 30 cm$\times$30 cm, in order to achieve a "flat response" (i.e., equally sensitive, see Fig. 10) over the central part of the field of view.

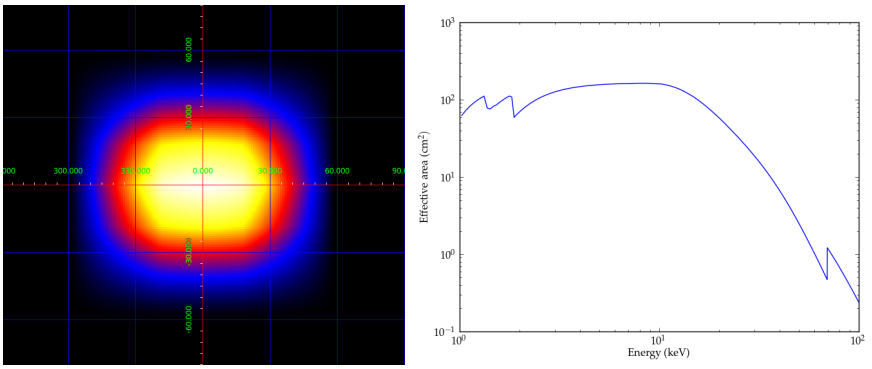

Fig. 10 Field of view of one of the four WFM units, and effective area as a function of energy.

As a baseline, due to telemetry limitations, the WFM will not operate in photon-by-photon mode at all times. Images in different energy ranges every 300 s, 0.1 keV resolution energy spectra every 30 s and light curves (bin size 16 ms) will be integrated and pre-processed by the BEEs and PDHU onboard (similar to what routinely done by Swift/BAT). A triggering algorithm will scan time series and images to detect fast transients, e. g., due to X-ray bursts or GRBs. Upon trigger, $\sim$300 s of photon-by-photon data will be downloaded to the telemetry. This mode of operation will provide the full achievement of

Parameter	Single Unit	Overall WFM
Energy range	2–50 keV (nominal)	2–50 keV (nominal)
Geometric Area	400 cm^2	1600 cm^2
Energy Resolution FWHM	<350 eV	<350 eV
FoV fully coded	0.40 sr	0.80 sr
FoV partially coded	2.90 sr	3.95 sr
Zero Response	118°	154°
Angular Resolution FWHM	$6' \times 7°$	$6' \times 6'$
Source Location Accuracy (10σ)	$< 1' \times 40'$	$< 1' \times 1'$
On-axis sensitivity at 5σ in 1 s	640 mCrab	450 mCrab
On-axis sensitivity at 5σ in 50 ks	2.9 mCrab	2.0 mCrab

Table 2 Performance of a single unit of the WFM and of the overall WFM

the primary science objective of the WFM: source monitoring and detection of interesting intensity and spectral states. Should a larger telemetry rate become available, photon data will be transmitted to the ground, enhancing the spectral and timing capabilities of this instrument.

The data processing requires an FPGA-based Back-End Electronics (BEE, one individual BEE for an orthogonal pair of units, as a redundancy) for the power DC/DC conversion and filtering, event cluster analysis, pedestal calculation and subtraction, time tagging, housekeeping, etc. The WFM total power consumption is estimated, including margin, as 12 W.

The telemetry packets of the WFM contain images, light-curves and energy spectra, accumulated on-board. The PDHU will reconstruct the event position and energy over the detector using the individual anode amplitude information, through proper algorithms and look-up tables. Upon trigger, the WFM data are sent to ground in photon-by-photon mode in dedicated telemetry packets. Total telemetry rate is estimated as 91 kbps (orbit average, before compression), including an average trigger rate of 1/day.

The overall WFM design includes 4 identical camera units assembled in a configuration where an orthogonal set of 2 cameras monitors the same sky region. The two sets are oriented at 37° to each other. The anticipated characteristics and performance of this WFM design and configuration are given in Table 2.

The WFM total volume is $4\times(30\times30\times15$ $cm^3)$, while the total mass, including 20% margin, is estimated as 37.0 kg.

5 LOFT Observing strategy and data flow

The LOFT mission will be operated by ESA as an observatory open to the general scientific community. The MOC and SOC are foreseen to be run by the ESA centers, while the science data center will be proposed at the ISDC

(Geneve). The latter will perform prompt and automated data screening in order to guarantee a proper prompt reaction to interesting transient events and source states.

The typical observing slots will last from a few ks to a few days, depending on the target and strategy. Given the characteristics of the LOFT scientific investigations, target of opportunity observations will be carried out, as triggered by the LOFT/WFM or by external triggers, in order to observe the variable sources in their most interesting and extreme physical states.

6 Summary and Conclusions

The LOFT mission proposal was selected by ESA as one of the four candidate M3 missions for the Cosmic Vision programme. ESA and the LOFT consortium will carry out an assessment phase of the mission over ∼18 months, concluding by the end of 2012. Further down-selections of the mission candidates are currently expected to bring only one of the four M3 candidates to a launch in the time-frame 2020-2022.

LOFT was primarily designed to address the fundamental questions raised by the Cosmic Vision under the "matter under extreme conditions" theme, through the study of the spectral and fast flux variability of compact X-ray sources. The high throughput required by this type of investigation is achieved by an unprecedented large collecting area: 15 m^2 geometric area, leading to 12 m^2 effective area peak at 6-10 keV (see Fig. 8), 20 times larger than any predecessors. The enabling technology is provided by the large area Silicon Drift Detectors and the capillary plate X-ray collimators, offering a large collecting and collimated area with limited resources in terms of mass, volume, power and costs. This type of detectors combine large area with very good spectral performance, enabling spectral studies with a resolution of ∼250 eV (FWHM). The segmentation of the Si drift detectors is a straightforward solution to the issues of dead time and pile-up, among the main problems in timing experiments.

Time variability from sub-ms to days will be explored by the LOFT LAD and WFM with statistical accuracy never achieved to date. For example, for the first time quasi-periodic oscillations in neutron star or black-hole systems will be studied in the time domain (as opposite to the frequency domain), within their coherence timescale. The large effective area and the spectral capabilities of LOFT will make optimal use of the diagnostic potential of the fast variability of the X-ray emission to probe the behaviour of matter in the strong gravity and ultradense environments, such as the innermost stable orbits around black holes or the interior of neutron stars, opening access to the understanding of the physical laws at work in such extreme conditions.

References

1. Abramowicz, M.A., Kluźniak, W.: A precise determination of black hole spin in GRO J1655-40. A&A **374**, L19–L20 (2001)
2. Bueno, J.I., García, I., Plaza, M.A.: SMOS PLM MIRAS hold-down release and deployment mechanisms. In: B. Warmbein (ed.) 11th European Space Mechanisms and Tribology Symposium, ESMATS 2005, *ESA Special Publication*, vol. 591, pp. 235–242 (2005)
3. Campana, R., Zampa, G., Feroci, M., Vacchi, A., Bonvicini, V., Del Monte, E., Evangelista, Y., Fuschino, F., Labanti, C., Marisaldi, M., Muleri, F., Pacciani, L., Rapisarda, M., Rashevsky, A., Rubini, A., Soffitta, P., Zampa, N., Baldazzi, G., Costa, E., Donnarumma, I., Grassi, M., Lazzarotto, F., Malcovati, P., Mastropietro, M., Morelli, E., Picolli, L.: Imaging performance of a large-area Silicon Drift Detector for X-ray astronomy. Nucl. Instr. Meth. A **633**, 22–30 (2011)
4. Demorest, P.B., Pennucci, T., Ransom, S.M., Roberts, M.S.E., Hessels, J.W.T.: A two-solar-mass neutron star measured using Shapiro delay. Nature **467**, 1081–1083 (2010)
5. Dovčiak, M., Bianchi, S., Guainazzi, M., Karas, V., Matt, G.: Relativistic spectral features from X-ray-illuminated spots and the measure of the black hole mass in active galactic nuclei. MNRAS **350**, 745–755 (2004)
6. Ebisawa, K., Bourban, G., Bodaghee, A., Mowlavi, N., Courvoisier, T.: High-energy sources before INTEGRAL. INTEGRAL reference catalog. ApJ **411**, L59–L62 (2003)
7. Fabian, A.C., Rees, M.J., Stella, L., White, N.E.: X-ray fluorescence from the inner disc in Cygnus X-1. MNRAS **238**, 729–736 (1989)
8. Feroci, M., Costa, E., Del Monte, E., Donnarumma, I., Evangelista, Y., Lapshov, I., Lazzarotto, F., Pacciani, L., Rapisarda, M., Soffitta, P., di Persio, G., Frutti, M., Mastropietro, M., Morelli, E., Porrovecchio, G., Rubini, A., Antonelli, A., Argan, A., Barbiellini, G., Boffelli, F., Bulgarelli, A., Caraveo, P., Cattaneo, P.W., Chen, A.W., Cocco, V., Colafrancesco, S., Cutini, S., D'Ammando, F., de Paris, G., Di Cocco, G., Fanari, G., Ferrari, A., Fiorini, M., Fornari, F., Fuschino, F., Froysland, T., Galli, M., Gasparrini, D., Gianotti, F., Giommi, P., Giuliani, A., Labanti, C., Liello, F., Lipari, P., Longo, F., Mattaini, E., Marisaldi, M., Mauri, A., Mauri, F., Mereghetti, S., Moretti, E., Morselli, A., Pellizzoni, A., Perotti, F., Piano, G., Picozza, P., Pilia, M., Pittori, C., Pontoni, C., Preger, B., Prest, M., Primavera, R., Pucella, G., Rappoldi, A., Rossi, E., Sabatini, S., Santolamazza, P., Tavani, M., Stellato, S., Tamburelli, F., Traci, A., Trifoglio, M., Trois, A., Vallazza, E., Vercellone, S., Verrecchia, F., Vittorini, V., Zambra, A., Zanello, D., Salotti, L.: Monitoring the hard X-ray sky with SuperAGILE. A&A **510**, A9 (2010)
9. Feroci, M., Costa, E., Soffitta, P., Del Monte, E., di Persio, G., Donnarumma, I., Evangelista, Y., Frutti, M., Lapshov, I., Lazzarotto, F., Mastropietro, M., Morelli, E., Pacciani, L., Porrovecchio, G., Rapisarda, M., Rubini, A., Tavani, M., Argan, A.: SuperAGILE: The hard X-ray imager

for the AGILE space mission. Nuclear Instruments and Methods in Physics Research A **581**, 728–754 (2007)
10. Gatti, E., Rehak, P.: Semiconductor drift chamber - An application of a novel charge transport scheme. Nuclear Instruments and Methods in Physics Research **225**, 608–614 (1984)
11. Giacconi, R., Kellogg, E., Gorenstein, P., Gursky, H., Tananbaum, H.: An X-Ray Scan of the Galactic Plane from UHURU. ApJ **165**, L27 (1971)
12. in't Zand, J.J.M., Weinberg, N.N.: Evidence of heavy-element ashes in thermonuclear X-ray bursts with photospheric superexpansion. A&A **520**, A81 (2010)
13. Israel, G.L., Belloni, T., Stella, L., Rephaeli, Y., Gruber, D.E., Casella, P., Dall'Osso, S., Rea, N., Persic, M., Rothschild, R.E.: The Discovery of Rapid X-Ray Oscillations in the Tail of the SGR 1806-20 Hyperflare. ApJ **628**, L53–L56 (2005)
14. Jahoda, K., Markwardt, C.B., Radeva, Y., Rots, A.H., Stark, M.J., Swank, J.H., Strohmayer, T.E., Zhang, W.: Calibration of the Rossi X-Ray Timing Explorer Proportional Counter Array. ApJS **163**, 401–423 (2006)
15. Kushpil, S., Crescio, E., Giubellino, P., Idzik, M., Kolozhvari, A., Kushpil, V., Martinez, M.I., Mazza, G., Mazzoni, A., Meddi, F., Nouais, D., Petráček, V., Piemonte, C., Rashevsky, A., Riccati, L., Rivetti, A., Tosello, F., Vacchi, A., Wheadon, R.: Beam test results of the irradiated silicon drift detector for ALICE. Nuclear Instruments and Methods in Physics Research A **566**, 94–99 (2006)
16. Laor, A.: Line profiles from a disk around a rotating black hole. ApJ **376**, 90–94 (1991)
17. Lattimer, J.M., Prakash, M.: Neutron Star Structure and the Equation of State. ApJ **550**, 426–442 (2001)
18. Lattimer, J.M., Prakash, M.: Neutron star observations: Prognosis for equation of state constraints. Physics Reports **442**, 109–165 (2007)
19. Leahy, D.A., Morsink, S.M., Chung, Y., Chou, Y.: Constraints on the Properties of the Neutron Star XTE J1814-338 from Pulse-Shape Models. ApJ **691**, 1235–1242 (2009)
20. Nouais, D., Beolè, S., Bondila, M., Bonvicini, V., Cerello, P., Crescio, E., Giubellino, P., Idzik, M., Kolozhvari, A., Kouchpil, S., Torres, E.L., Martinez, M.I., Mazza, G., Piano, S., Piemonte, C., Rashevsky, A., Riccati, L., Rivetti, A., Tosello, F., Trzaska, W.H., Vacchi, A., Wheadon, R., The ALICE Collaboration: The ALICE Silicon Drift Detector system. Nuclear Instruments and Methods in Physics Research A **501**, 119–125 (2003)
21. Peacock, A., Andresen, R.D., Manzo, G., Taylor, B.G., Villa, G., Re, S., Ives, J.C., Kellock, S.: The gas scintillation proportional counter on EXOSAT. Space Science Reviews **30**, 525–534 (1981)
22. Plaza, M.A., Martinez, L., Cespedosa, F.: The development of the SMOS-MIRAS deployment system. In: R. A. Harris (ed.) 10th European Space Mechanisms and Tribology Symposium, *ESA Special Publication*, vol. 524, pp. 231–238 (2003)
23. Rashevsky, A., Bonvicini, V., Burger, P., Piano, S., Piemonte, C., Vacchi,

A.: Large area silicon drift detector for the ALICE experiment. Nuclear Instruments and Methods in Physics Research A **485**, 54–60 (2002)
24. Shvartsman, V.F.: Neutron Stars in Binary Systems Should Not Be Pulsars. Soviet Ast.**15**, 342 (1971)
25. Stella, L., Vietri, M., Morsink, S.M.: Correlations in the Quasi-periodic Oscillation Frequencies of Low-Mass X-Ray Binaries and the Relativistic Precession Model. ApJ **524**, L63–L66 (1999)
26. Strohmayer, T.E., Watts, A.L.: Discovery of Fast X-Ray Oscillations during the 1998 Giant Flare from SGR 1900+14. ApJ **632**, L111–L114 (2005)
27. Swank, J.H.: The Rossi X-ray timing explorer: Capabilities, achievements and aims. Advances in Space Research **38**(1), 2959–2963 (2006)
28. Taylor, B.G., Andresen, R.D., Peacock, A., Zobl, R.: The EXOSAT mission. Space Sci. Rev.**30**, 479–494 (1981). DOI 10.1007/BF01246069
29. Turner, M.J.L., Thomas, H.D., Patchett, B.E., Reading, D.H., Makishima, K., Ohashi, T., Dotani, T., Hayashida, K., Inoue, H., Kondo, H., Koyama, K., Mitsusa, K., Ogawara, Y., Takano, S., Awaki, H., Tawara, Y., Nakamura, N.: The large area counter on GINGA. PASJ **41**, 345–372 (1989)
30. Vacchi, A., Castoldi, A., Chinnici, S., Gatti, E., Longoni, A., Palma, F., Sampietro, M., Rehak, P., Kemmer, J.: Performance of the UA6 large-area silicon drift chamber prototype. Nucl. Instr. Meth. A **306**, 187–193 (1991)
31. van der Klis, M.: Millisecond Oscillations in X-ray Binaries. ARA&A **38**, 717–760 (2000)
32. Zampa, G., Campana, R., Feroci, M., Vacchi, A., Bonvicini, V., Del Monte, E., Evangelista, Y., Fuschino, F., Labanti, C., Marisaldi, M., Muleri, F., Pacciani, L., Rapisarda, M., Rashevsky, A., Rubini, A., Soffitta, P., Zampa, N., Baldazzi, G., Costa, E., Donnarumma, I., Grassi, M., Lazzarotto, F., Malcovati, P., Mastropietro, M., Morelli, E., Picolli, L.: Room-temperature spectroscopic performance of a very-large area silicon drift detector. Nucl. Instr. Meth. A **633**, 15–21 (2011)